Al Azhar Bulletin of Science Vol. 29, No. 2 (December), 2018, pp. 157-166

APPLICATION OF MAGNETITE NANOPARTICLES FOR ADSORPTION OF ACID RED 141 FROM AQUEOUS SOLUTIONS.

Abeer A. Emam, Gomaa S.H, ELsisi A.A, Emam A.G.

Department of Chemistry, Faculty of Science, Al-Azhar University (Girls), Nasr City, Cairo, Egypt.

ABSTRACT

The potential of Fe_3O_4 magnetic nanoparticles (MNPs) as efficient adsorbent for acid red 141, as anionic dye, from aqueous solutions was investigated. For this purpose, Fe_3O_4 MNPs were synthesized via chemical co-precipitation method. The synthesized MNPs were characterized by SEM, FT-IR, XRD, and EDX techniques. The various parameters affecting dye adsorption were investigated and optimized. The kinetic studies for acid red 141 adsorption showed rapid sorption dynamics by second-order kinetic model. Dye adsorption equilibrium data were fitted well to the Freundlich isotherm rather than Langmuir isotherm. The over all adsorption process was favorable, exothermic, and follows both intraparticle and Elovich diffusion models. Maximum capacity (q_{max}) was calculated, and was found to be 700 mg/g at 10°C and 985 mg/g at 50°C. The results showed that magnetic nanoparticles could be employed as a low-cost efficient adsorbent for removal of anionic dyes from aqueous solution.

Keywords: Adsorption percent (%), adsorption capacity (q_e), Acid Red 141, magnetite nanoparticles (MNPs), SEM, EDX, XRD, FT-IR.

1. INTRODUCTION

Dyes have been extensively used for thousands of years for textile, paint, pigment, and many other applications [1]. Today dyes play a critical role in textile, paint, and pigment manufacturing industries, where at least 100,000 different dye types are currently commercially available [2]. To meet industrial demand, it is estimated that 1.6 million tons of dyes are produced annually, and 10-15% of this volume is discarded as wastewater [3]; as a result dyes are major water pollutants. Excessive exposure to dyes cause skin irritation, respiratory problems, and, for some dyes, increases cancer risk in humans [4]. In addition, the presence of dye in wastewater also contributes to high chemical oxidation demand, and causes foul odour [5]. Thus, it is of utmost importance to remove dyes from wastewater effectively to ensure safe discharge of treated liquid effluent into water resources.

Typically, dye wastewater is treated using coagulation–flocculation [6], aerobic or anaerobic treatment [7], electrochemical treatment [8], membrane filtration [9], and adsorption methods [10]. Adsorption is the most popular of these methods due to the effectiveness and the simplicity of the process. Low-cost adsorbents derived from solid and agricultural wastes have received widespread attention from researchers in the last decade [11]. However, most of these low-cost adsorbents are micro particles [12], whose small contact surface area requires considerable time to achieve maximum adsorption of pollutants. As most industries require a fast adsorption rate to sustain increasing pollutant capacities, developing these adsorbents for industrial applications is not feasible. Therefore, the need to develop sustainable adsorbents that are economical, and offer both high adsorption rates and high adsorption capacities is urgent.

Nanomaterials, also referred to as nanoparticles, are particles that fall within the size range of 1–100 nm. Generally, well known nanomaterials are valued for their strength, highly active sites, and low mass [13]. Some nanomaterials have two main advantages: they can be easily synthesized at a low cost, and small amounts are required for effective adsorption of pollutants [14]. Thus, it is expected that nanomaterials will become more economical for adsorption applications.

Magnetic nanoparticles (MNPs) are a class of nanoparticles, which have been found to have low toxicity on humans, and can be manipulated using a magnetic field. MNPs have the advantages of large surface area, high number of surface active sites, and high magnetic properties, which cause high adsorption efficiency, high adsorption rate of contaminants, and easy and rapid separation of adsorbent from solution via magnetic field. After magnetic separation, the contaminants can be easily removed from nanoparticles by the desorbent agents, and the recovered MNPs can be reused [15,16]

The aim of this present work is to describe the chemical synthesis, characterization, and applicability of Fe_3O_4 MNPs as an efficient adsorbent for adsorption of acid red 141 (AR 141) from aqueous samples. The different parameters related to adsorption, isotherm, kinetics, and diffusion are evaluated and discussed.

2. EXPERIMENTAL

2.1. Reagents and materials

Acid red 141 ($C_{20}H_{13}N_2NaO_4S$), shown in Figure 1 as an anionic dye, ferric chloride ($FeCl_3$. $6H_2O$), ferrous chloride ($FeCl_2.4H_2O$), sodium hydroxide, and hydrochloric acid were purchased with high purity from Merck (Darmstadt, Germany). A stock standard solution of AR 141 at a concentration of 1000 ppm was prepared in double distilled water. This standard solution was diluted with doubly distilled water to prepare series of solutions with the concentration of 40, 80, 120, 160, and 200 ppm of AR 141.

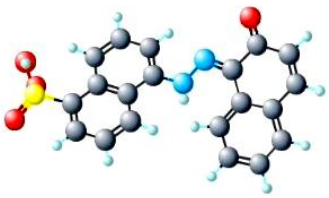

Figure 1. Molecular structure of 3D Conformer of Parent Acid Red 141 (AR141)

2.2. Synthesis of Fe_3O_4 magnetic nanoparticles

Fe_3O_4 MNPs were prepared by chemical coprecipitation method [17] in a three-necked reactor. Firstly, 10.4 g of $FeCl_3.6H_2O$, 4.0 g of $FeCl_24H_2O$, and 1.7 mL of 12 mol L^{-1} HCl were dissolved in 50 mL of deionized water in a beaker, which was degassed with nitrogen gas for 20 minutes before use, to prepare a stock solution of ferrous and ferric ions. On the other hand, 500 mL of 1.5 mol L^{-1} NaOH solution was degassed for 15 minutes, and heated to $80^{\circ}C$ in the reactor. Then, the stock solution of ferrous and ferric ions was added drop wise, using a dropping funnel, during 30 minutes under nitrogen gas protection and vigorous stirring by the use of the glassware stirrer. During the whole process, the solution temperature was maintained at $80^{\circ}C$, and nitrogen gas was used to prevent the intrusion of oxygen. The obtained Fe_3O_4 powder was subsequently removed from the solution via centrifugation, and resuspended in 500 mL of degassed deionized water. The obtained MNPs were stable in this condition up to one month.

2.3. Adsorption of Acid Red 141 using synthesized MNPs

In primary experiments the adsorption behavior of acid red 141 at various pHs was studied by measuring the absorbance of solutions at 509 nm. To achieve maximum adsorption efficiency, various parameters affecting the dye adsorption were studied and optimized. Optimization studies were carried out according to the following procedure: (1) 50 mL aqueous solution of the dye (80 ppm) was poured in a conical flask, (2) 200 mg of Fe_3O_4 MNPs was added to the dye solution, (3) pH of the solution was adjusted to the desired value, (4) the mixture was stirred for 120 minutes, (5) after dye adsorption, Fe_3O_4 MNPs were quickly separated from the sample solution (6) the residual dye concentration in the supernatant clear solution was determined spectrophotometrically by UV-vis spectrophotometer (Perkin Elmer Lambda 35, USA).

2.3.1. Adsorption %

The following equation was applied to calculate the dye adsorption %

$$\%Adsorption = \frac{C_o - C_e}{C_o} \times 100$$

Where C_o and C_e are the initial and final concentrations of the dye in the solution respectively.

2.3.2. Adsorption capacity (q_e)

Adsorption capacity q_e(mgg^{-1}) after equilibrium was calculated by a mass balance relationship as follows:

$$qe = (C_o - C_e)\frac{V}{W}$$

where C_o is the initial and C_e is the final equilibrium concentrations of the test solution, V is the volume of the solution, and W is the mass of adsorbent (mg).

3. RESULTS AND DISCUSSION

3.1. Characterization and Analysis:

3.1.1. *SEM and EDX*

SEM image was a cquisited to determine the morphology and particle size of the adsorbent Fe_3O_4MNPs (Fig. 2(a)) where the nanoparticles were obtained to be spherical and of average size of 20 nm with narrow size distribution.

The EDX analysis (Fig. 2b), shows that the nanoparticles consist of Fe and O elements. Results from Table 1 confirms the appearance of Fe_3O_4 nanoparticles.

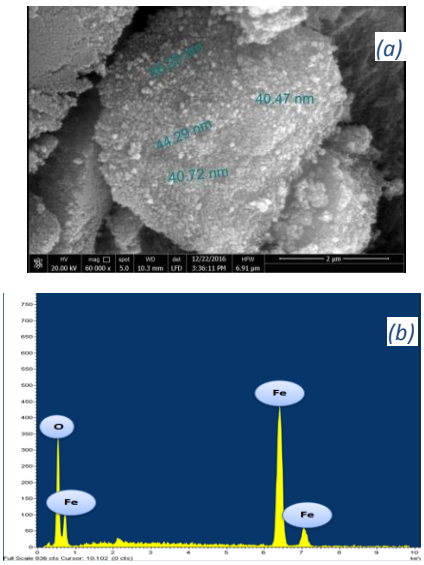

Figure 2. (a) SEM image and (b) EDX mapping of the Fe_3O_4 MNPs

Table 1.Persentage of elements in Fe_3O_4 nanoparticles.

Element	Weight%	Atomic%
CK	7.16	15.07
O K	38.69	61.11
Fe K	52.02	61.11
Au M	2.12	0.27
Totals	**100.00**	

3.1.2. FT-IR Analysis

The FT-IR spectra were recorded to prove the successful preparation of AR141 loaded MNPs and possible interaction between various constituents of nanoparticles. FT-IR spectrum of the MNPs (a), AR141 coated MNPs (b), are shown in Fig. 3 The strong absorption at 584 cm^{-1} in curves a and b are attributed to the stretch of Fe-O, and the broad absorption peak appeared at about 3395 cm^{-1} can be related to the presence of hydroxyl groups. Comparing spectra a and b, some new absorption bands are appeared. For instance, the bands at about 1028and 1155 cm^{-1} were due to the stretching vibration of the alcoholic hydroxyl (C–O), and the band at 1466 cm^{-1} was attributed to the bending vibration of C–H bond. These data proved that the surface of MNPs has been covered with AR141. It is believed that different interactions such as van der Waals force, hydrogen bond, and electrostatic interactions keep AR141 on the surface of MNPs. A similar pattern could also be observed in the spectrum of Fe_3O_4-AR141, which indicates that the AR141 was successfully loaded onto the Fe_3O_4 MNPs.

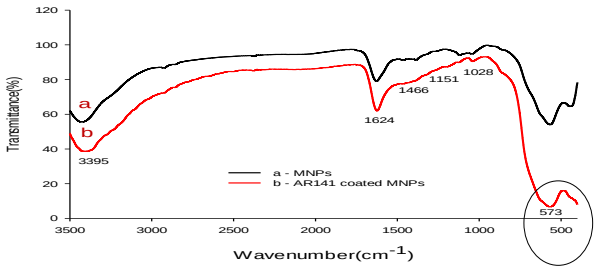

Figure 3. FT-IR spectra of MNPs (a), **AR141**coated MNPs (b)

3.1.3. XRD Analysis

The crystal structure of nano-Fe3O4 was characterized using XRD for 2θ diffraction angles from 20° to 60°. As shown in Figure 4, the sharp peaks at 30.124°, 35.476°, 43.135°, 53.506°, and 56.991° in the XRD pattern are matches well with the reported standard pattern (JCPDS No.75-1372). The diffraction peaks are quite sharp and no peaks for impurities are detected. The results show the sample is nano-Fe3O4 which has high purity and well-crystallizes structure.

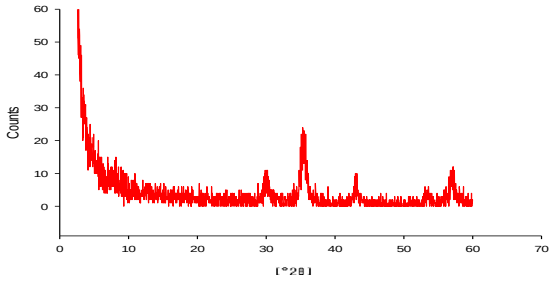

Figure 4: XRD pattern of the Fe_3O_4 nano-particles

3.2. Parametric studies

The adsorption of Acid red 141 is studied at λ_{max} 509 nm. The optimum condition for adsorption of AR 141 is 80 ppm, pH 3, and Fe_3O_4 MNPs dose of 200 mg. The results obtained during this study are as shown below.

3.2.1. Influence of pH

The adsorption of AR 141 was studied at different pH values, as it is an important parameter for the reaction taking place on the particular surface. The pH range was from 1.5-10. According to the data in Table 2, it was found that the adsorption % and adsorption capacity (q_e) of AR 141 are high in acidic solutions due to electrostatic attractions between the dye, in its anionic form, and the positively charged surface of Fe_3O_4 MNPs. When the solution pH was increased from 1.5 to 10, adsorption % was decreased. This can be explained by considering both the pHpzc of the adsorbent as well as the molecular nature of AR 141 [18]. Beyond pHpzc, negative charges develop on the surface of adsorbent causing a decrease in the number of positively charged sites; moreover, repulsion of the dye anions was observed [18] leading to minimum value of 25% removal at pH 10.

3.2.2. Effect of adsorbent dosage

As adsorbent dosage increases, keeping all the other parameters at constant values, adsorption efficiency firstly increases, reaches maximum, and then decreases, due to the availability of the exchangeable active sites of the MNPs [19]. With the increase in adsorbent dose, aggregation of particle takes place. The optimum adsorbent mass was selected to be 200 mg, achieving 94.47% adsorption after 45 minute at 20℃ , as shown in Table 2.

3.2.3. Effect of initial concentration of AR141

The effect of initial concentration (ppm) on the adsorption % and adsorption capacity (q_e) of AR 141 by MNPs is shown in Table (2). Initial concentration was varied from 40, 80, 120, 160 to 280 ppm. Time, pH, adsorbent dosage, and temperature were kept constant. It can be seen from the results that the adsorption % decreased gradually upon increasing the AR 141 concentration. Sufficient adsorption sites are available at lower initial concentrations, but at higher concentrations dye ions are greater than adsorption sites [20]. Thus, it can be concluded that adsorption of dye is concentration dependent using MNPs.

Table 2. Influence of pH, adsorbent dose, and dye concentration on the adsorption % and adsorption capacity (q_e) of AR 141 on MNPs at 20°C.

pH			Adsorbent dose			Dye concentration		
pH	%	q_e (mg g^{-1})	Dose (mg)	%	q_e (mg g^{-1})	ppm	%	q_e (mg g^{-1})
1.5	80.60	303.33	50	42.11	200.12	40	95.10	477.13
2.0	88.51	365.12	100	63.16	300.45	80	94.47	450.34
3.0	94.47	450.34	150	78.94	375.95	120	88.42	420.11
4.0	72.15	305.22	200	94.47	450.12	160	76.00	362.50
6.0	50.80	206.14	225	47.36	225.34	200	63.15	300.00
8.0	33.06	108.16	250	31.58	150.45	240	58.16	242.13
10.0	25.15	53.56	275	20.18	43.12	280	52.01	203.34

3.2.4. Effect of contact time

As the time of adsorption is changed from 5 to 120 minutes, efficiency firstly increased, and afterwards no change is observed. As time progresses the surface coverage of the adsorbent is high, and further no adsorption takes place. Figure 5 shows the effect of time on adsorption capacity. According to these results, the agitation time was fixed at 1 hour for the rest of the batch experiments to make sure that equilibrium was attained, which is considered adequate and economical for wastewater treatment [21].

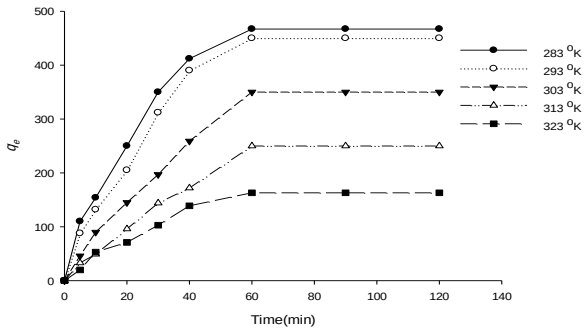

Figure 5: Effect of contact time on the adsorption capacity (q_e) of AR 141 on MNPs at different temperatures. (C_{dye} = 80 ppm, pH = 3.0, adsorpent dose = 200.0mg) .

3.3. Adsorption isotherms

Adsorption isotherm models are widely used to describe and investigate mechanisms of adsorption. The equilibrium data was analyzed by the Langmuir and Freundlich isotherm models.

3.3.1. Langmuir model

The linear form of Langmuir equation can be written as follows:

$$\frac{C_e}{Q_e} = \frac{C_e}{Q_m} + \frac{1}{K_L Q_m}$$

where C_e (mgL^{-1}) is the concentration of AR 141 at equilibrium, Q_e (mgg^{-1})is the amount of AR 141 adsorbed by the MNPs at equilibrium, Q_m (mgg^{-1}) is the maximum adsorption capacity corresponding to monolayer coverage, and R_L (L/mg) is the Langmuir constant. The values of Q_m and R_L can be calculated from plotting C_e /Q_e versus C_e. In order to determine if the adsorption process is favorable or unfavorable, a dimensionless constant, separation factor or equilibrium parameter R_L, is defined according to the following equation.

$$R_L = \frac{1}{1 + K_L C_o}$$

where K_L (L/mg) is the Langmuir constant and C_e (mg/L) is the initial AR 141 concentration. The R_L value indicates adsorption process is irreversible when R_L is 0; favorable when R_L is between 0 and 1; linear when R_L is 1; and unfavorable when R_L is greater than 1 [22].

The Langmuir plots for AR 141 adsorption on MNPs are obtained in Figure 6, and the parameters are shown in Table 3. The values of the correlation coefficient for the Langmuir plots changed in the range 0.5504-0.8349. This suggests that the adsorption of AR 141 on MNPs did not follow the Langmuir model at the five temperatures. The calculated values of R_L are all in the range of 0.013-0.063; thereby, confirming that the five adsorption processes at (10, 20, 30, 40, and 50℃) are all favorable [23].

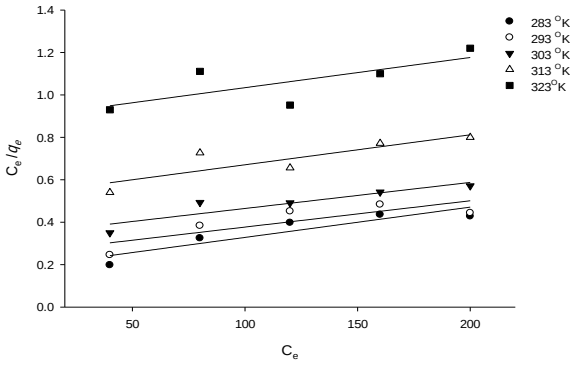

Figure 6: Fitting of isotherm data to the Langmuir model of AR141 on MNPs at different temperatures. (pH = 3,0, adsorpent dose = 200.0mg).

3.3.2. Freundlich model

The linear form of Freundlich equation is given as:

$$\log Q_e = \log K_F + \frac{1}{n} \log Ce$$

where Q_e is the AR141 concentration on MNPs at equilibrium, C_e (mgL^{-1}) is the concentration of AR141 in solution at equilibrium, and K_F (dm^3g^{-1}) and 1/n are Freundlich constants related to adsorption capacity and adsorption

intensity, respectively [23]. Freundlich constants are calculated from the slope and the intercept in Figure 7, and are given in Table 3. The correlation coefficients ($r^2 > 0.925$) reflect that the experimental data agree well with the Freundlich model. The values of 1/n (0.498, 0.632, 0.713, 0.778, and 0.868 at 283, 293, 303, 313, and 323° K respectively) are all smaller than 1, so they represent the favorable adsorption conditions [24].

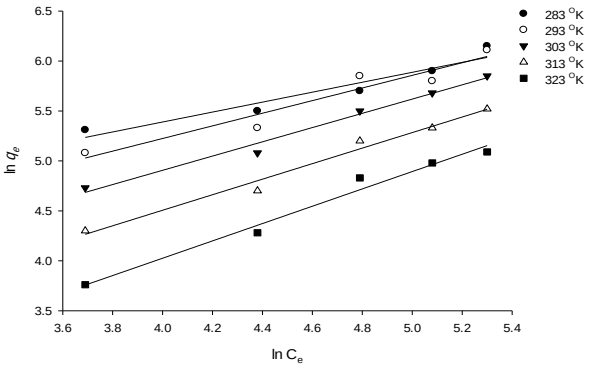

Figure 7: Fitting of isotherm data to the Freundlich model of AR 141 on MNPs at different temperatures. (pH = 3.0, adsorpent dose = 200.0 mg)

3.4. Adsorption kinetics

In order to examine the mechanism and rate-controlling step in the overall adsorption process, four kinetic models, pseudo-first-order, pseudo-second-order, intraparticle diffusion, and Elovich diffusion, are adopted to investigate the adsorption process.

3.4.1.Pseudo-first order

The pseudo-first-order equation can be expressed as in the following equation:

$$\log (q_e - q_t) = \log q_e - \frac{k_1}{2}, 303\ t.$$

where q_e and q_t (mgg^{-1}) are the AR 141 adsorption capacity at equilibrium and at time t (minutes) respectively, and k_1 (min^{-1}) is the rate constant of the pseudo-first-order. The parameters k_1 and q_e could be calculated from the slope and intercept of the plots of log ($q_e - q_t$) versus t, and are found to be unbeseeming for the present system. This suggests that the pseudo-first-order kinetic model is not suitable to describe the adsorption process.

3.4.2.Pseudo-second order kinetic model

The pseudo-second order kinetic model can be expressed in linear form as follows:

$$\frac{t}{q_t} = \frac{1}{k_2 q_e^2} + \frac{t}{q_e}$$

Where k_2 (g/mg min) is the pseudo-second-order rate constant. The q_e and k_2 values can be obtained from the slope and intercept of plots of t/q_t versus t, which are illustrated in Figure 8. The good linear plots of t/q_t versus t at different temperatures, along with the correlation coefficients r^2 higher than 0.900 suggest that adsorption of AR141 on MNPs predominantly follows the pseudo-second order kinetic model [20]. The parameters, k_2 and q_{max}, are listed in Table 4. The values of the adsorption capacity at equilibrium (q_{max}) for AR141 are decreased

Table 3: Langmuir and Freundlich isotherm constants, correlation coefficients, and separation factors for the adsorption of AR 141 on MNPs at various temperatures.

T (°K)	Langmuir constants			Freundlich constants			Separation factor (b)
	q_{max}(mgg^{-1})	K_{Lx10^3} (dm^3g^{-1})	r_L^2	1/n	$K_{F(dm^3g^{-1})}$	r_F^2	
283	700.88	7.68	0.83	0.49	29.93	0.93	0.063
293	806.45	4.89	0.69	0.63	14.82	0.93	0.047
303	814.99	3.58	0.83	0.71	12.67	0.98	0.035
313	898.71	2.10	0.73	0.78	4.03	0.98	0.023
323	985.74	1.12	0.55	0.87	1.74	0.98	0.013

Table 4: Pseudo-second-order kinetic parameters for the adsorption of AR141 onto MNPs at various temperatures.

T (^oK)	K_2 x 10^4 ($g\ mg^{-1}min^{-1}$)	q_{max} (mg g^{-1})	r^2
283	1.0	595.24	0.976
293	1.55	537.63	0.944
303	1.73	452.48	0.922
313	1.81	337.84	0.948
323	1.92	204.92	0.902

from 595.24 to 204.92 mgg^{-1} when the temperature is increased from 283 to 323° K. This effect can be explained by assuming that at higher temperatures the total energy of the adsorbate species is increased, and their escaping tendency fro

m the adsorbent surface is also increased; therefore the adsorption of the adsorbate species is decreased. This suggests that the lowest temperature favours AR141 adsorption, and the adsorption equilibrium capacity is dependent on temperature [25].

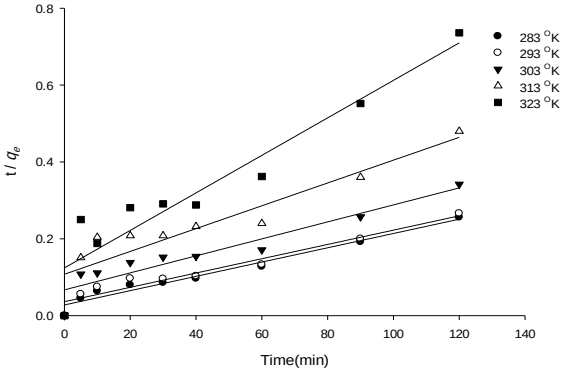

Figure 8: Fitting of the kinetic data to the pseudo-second order kinetic model of AR141 on MNPs at different temperatures. (C_{dye} = 80 ppm, pH = 3.0, adsorpent dose = 200.0 mg)

The pseudo-second order rate constants for adsorption of AR141 on MNPs system show a steady increase with temperature, as shown in Table 3. The values of the rate constants were found to increase from 1.0 x 10^{-4} to 1.92 x 10^{-4} g $mg^{-1}min^{-1}$, with an increase in the solution temperature from 283 to 323° K. In conventional physisorption systems, increasing the temperature usually increases the rate of approach to equilibrium, but decreases the equilibrium capacity.

3.4.3. Arrhenius activation energy of adsorption process

The pseudo-second-order rate constant of dye adsorption is expressed as a function of temperature by the Arrhenius relationship:

$$\ln k_2 = \ln A - \frac{E_a}{RT}$$

where E_a is the Arrhenius activation energy representing the energy barrier that a dye species should overcome to be adsorbed into the MNPs [26]. The magnitude of activation energy gives an idea about the type of adsorption, which is mainly physical or chemical. The physisorption processes usually have energies in the range of 5-40 kJ mol^{-1}, while higher activation energies (40-800 kJ mol^{-1}) suggest chemisorptions [27]. The value is found to be in the typical activation energy range for physisorption, thus it can be concluded that AR141 is mainly physically adsorbed on MNPs surface.

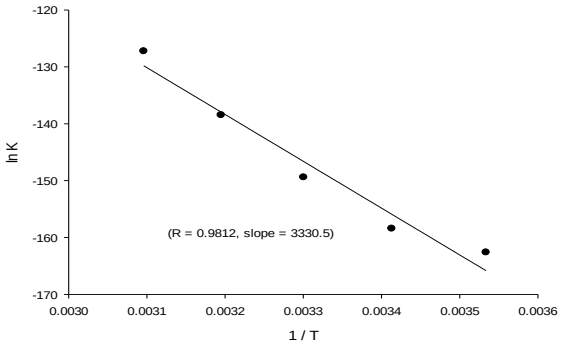

Figure 9: Arrhenius plot for the adsorption of AR 141 on MNPs

3.5.diffusion mechanism

The two models above cannot identify the diffusion mechanism during the adsorption process, so the experimental data are tested by the intraparticle diffusion model, and Elovich diffusion model.

3.5.1.Intraparticle diffusion model

Intra-particle diffusion can be expressed by following equation:

$$q_t = k_p t^{1/2} + C$$

where q_t (mg/g) is the amount of AR 141 adsorbed at time t (minutes), k_p (mg/g $min^{1/2}$) is the intraparticle diffusion rate constant, and C is the intercept. The plot of q_t versus $t^{1/2}$, in Figure 10, shows a double straight line nature [28]. The first linear part could be due to the entry of AR141 species into the MNPs particle by intraparticle diffusion. The second horizontal linear part represents the final equilibrium stage. As given in Table 5, it is obvious that the values of k_p decrease from 46.67 to 17.42 mg/g $min^{1/2}$ when the temperature increases from 283 to 323° K

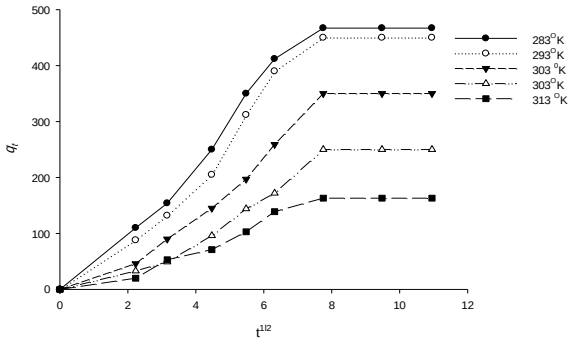

Figure 10: Intraparticle diffusion model of AR141 on MNPs at different temperatures. (C_{dye} = 80 ppm, pH = 3.0, adsorpent dose = 200.0 mg)

3.5.2. Elovich-diffusion model

The *Elovich* equation is often valid for systems in which the adsorbing surface is heterogeneous [29]. The equation is given as follow

$$q_t = \left(\frac{1}{\beta}\right) ln\,\alpha\beta + \left(\frac{1}{\beta}\right) ln\,t$$

where α is the initial adsorption rate constant (mg/g min), and β is the desorption constant (g/mg) during any one experiment. The constants can be obtained from the slope and the intercept of the plot of q_t versus $ln\,t$ at different temperatures, as shown in figure 11. The value of β increases from 7.66 to 19.83 $x10^{-3}$ (g/mg), as shown in table 5.

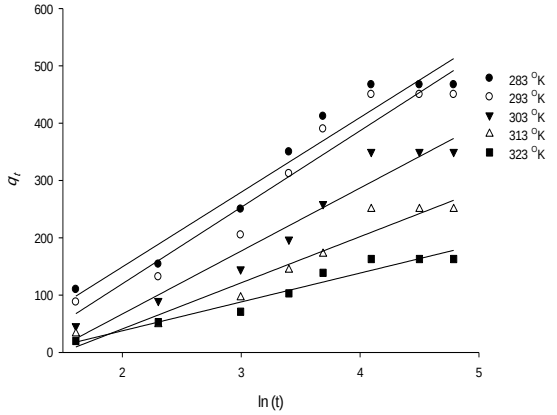

Figure 11: Elovich adsorption model of AR 141 on MNPs at different temperatures. . (C_{dye} = 80 ppm, pH = 3.0, adsorpent dose = 200.0 mg)

CONCLUSION

1. MNPs are successfully synthesised through coprecipitation method, and can be used as an efficient and cheap adsorbent for the removal of acid red 141 dye from aqueous solution.
2. Adsorptive removal of acid red 141 dye by using adsorbent dose 200 mg is successfully applied and optimized; while with an increasing dye concentration, the adsorption rate decreases. Acidic pH condition significantly affects the dye adsorption efficiency of acid red 141 dye, and was found to be 94.47 % at pH 3.
3. Lowering the temperature favors adsorption, due to the higher escaping tendency of adsorbate species as the temperature rises.
4. The amount of adsorbed dye is increased with an increase of contact time, which was optimized at 60 minutes, and the rate of adsorption is found to confirm the pseudo-second-order kinetic model with good values of correlation coefficient.
5. Adsorption isotherms are described by Langmuir and Freundlich isotherm models. Freundlich isotherm model is found to fit with experimental data due to higher r^2 values
6. Intraparticle diffusion model and Elvoich model have good correlation with r^2 values,

which indicates their applicability to the system.

REFERENCES

[1] J. Liu, D. Guo, Y. Zhou, Z. Wu, W. Li, F. Zhao, X. Zheng, Identification of ancient textiles from Yingpan, Xinjiang, by multiple analytical techniques, J. Archaeol.Sci. 38 (2011) 1763–1770.

[2] V.K. Gupta, Suhas, Application of low-cost adsorbents for dye removal – a review, J. Environ. Manage. 90 (2009) 2313–2342.

[3] Hunger, Industrial Dyes – Chemistry, Properties, Application, Wiley, 2003.

[4] H.S. Rai, M.S. Bhattacharyya, J. Singh, T.K. Bansal, P. Vats, U.C. Banerjee, Removal of dyes from the effluent of textile and dyestuff manufacturing industry: a review of emerging techniques with reference to biological treatment, Crit. Rev. Environ. Sci. Technol. 35 (2005) 219–238.

[5] V. Midha, A. Dey, Biological treatment of tannery wastewater for sulfide removal J. International, Chem. Sci. 6 (2009) 472–486.

[6] J. García-Montaño, X. Domènech, J.A. García-Hortal, F. Torrades, J. Peral, The testing of several biological and chemical coupled treatments for Cibacron Red FN-R azo dye removal, J. Hazard. Mater. 154 (2008) 484–490.

[7] E. Hosseini Koupaie, M.R. Alavi Moghaddam, S.H. Hashemi, Post-treatment of anaerobically degraded azo dye Acid Red 18 using aerobic moving bed biofilm process: enhanced removal of aromatic amines, J. Hazard. Mater. 195 (2011)147–154.

[8] B.K. Körbahti, K. Artut, C. Geçgel, A. Özer, Electrochemical decolorization of textile dyes and removal of metal ions from textile dye and metal ion binary mixtures, Chem. Eng. J. 173 (2011) 677–688.

[9] E. Alventosa-deLara, S. Barredo-Damas, –M.I. Alcaina-Miranda, M.I. Iborra-Clar,

Ultrafiltration technology with a ceramic membrane for reactive dye removal: optimization of membrane performance, J. Hazard. Mater. 209–210 (2012) 492500.

[10] G. Zhang, L. Yi, H. Deng, P. Sun, Dyes adsorption using a synthetic carboxy methyl cellulose-acrylic acid adsorbent, J. Environ. Sci. 26 (2014)1203–1211.

[11] M.S.U. Rehman, I. Kim, J.I. Han, Adsorption of methylene blue dye from aqueous solution by sugar extracted spent rice biomass, Carbohydr. Polym.90 (2012) 1314–1322.

[12] B.R. Müller, Effect of particle size and surface area on the adsorption of albumin-bonded bilirubin on activated carbon, Carbon 48 (2010) 3607–3615.

[13] M.J. Sweet, A. Chessher, I. Singleton, Review: metal-based nanoparticles; size, function, and areas for advancement in applied microbiology, Adv. Appl. Microbiol. 80 (2012) 113–142.

[14] Y.H. Chen, Synthesis, characterization and dye adsorption of ilmenite nanoparticles, J. Non-Cryst. Solids 357 (2011) 136–139.

[15] Oliveira, L.C.A., Rios, R.V.R.A., Fabris, J.D., Sapag, K., Garg, V.K.,Lago, R.M.Clay-iron oxide magnetic composites for the adsorption of contaminant in water. Appl. Clay Sci. 22(2003) 169–177.

[16] Fereshte Keyhanian, Shahab Shariati, Mohammad Faraji, Maryam Hesabi.Magnetite nanoparticles with surface modification for removal of methyl violet from aqueous solutions . Arabian Journal of Chemistry ,9, (2016) S348–S354

[17] Zhao, X., Shi, Y., Wang, T., Cai, Y., Jiang, G., Preparation of silica-magnetite nanoparticle mixed hemimicelle sorbents for extraction of several typical phenolic compounds from environmental water samples. J. Chromatogr. A 1188(2008) 140

[18] Stevan Luther, Nathan Borfeld, Jisoo Kim, Parsons JG. Removal of arsenic from aqueous solution: A study of the effects of pH and interfering ions using iron oxide nanomaterials. Microchemical Journal:101(2012)30-36

[19] Amira M. Mahmoud, Fatma A. Ibrahim, Seham A. Shab, Nadia A. Youssef. Adsorption of heavy metal ion from aqueous solution by nickel oxide nano catalyst prepared by different methods Egyptian Journal of Petroleum, 24(2015), 27–35.

[20] Manohar R. Patil and V.S. Shrivastava Adsorption removal ,of carcinogenic acid violet 19 dye from aqueous solution by polyaniline-Fe_2O_3 magnetic nano-composite, J.Mater Environ Sci, 6 (1) (2015) 11-21.

[21] K. Kadirvelu, C. Namasivayam, Activated carbon from coconutcoirpith as metal adsorbent: adsorption of Cd (II) from aqueous solution, Adv. Environ. Res., 7 (2003) 471–478.

[22] Frédéric Gimbert, Nadia Morin-Crini, François Renault, Pierre-Marie Badot, Grégorio Crini. Adsorption isotherm models for dye removal by cationized starch-based material in a single component system, j. of Hazardous Materials. 157, 1 (30) (2008) 34–46.

[23] Mahmoudi Z., Azizian S., Lorestani B. Removal of methylene blue from aqueous solution: A comparison between adsorption by iron oxide nanospheres and ultrasonic degradation J. Mater. Environ. Sci. 5 (5) (2014) 1332-1335.

[24] Padmavathy K. S.a, G.Madhub, Haseena. P.V.a. A study on effects of pH, adsorbent dosage, time, initial concentration and adsorption isotherm study for the removal of hexavalent chromium (Cr (VI)) from wastewater by magnetite nanoparticles Procedia Technology 24 (2016) 585 – 594.

[25] PengLuoa, B, Yafei Zhao A, Bing Zhang A, Jindun Liu A, Yong Yang B, Junfang Liub, water research Study on the adsorption of Neutral Red from aqueous solution onto halloysite nanotubes, 4 4 (2010) 1489 – 1497.

[26] Kim, T.K, Y.A. Son, Y.J. Lim, Thermodynamic parameters of disperse dyeing on several polyester fibers having different molecular structures. Dyes Pigm., 67: (2005) 229-234.

[27] Nollet, H., M. Roels, P. Lutgen, P.V. Meeren, W. Verstraete, Removal of PCBs from wastewater using fly ash, Chemosph., 53: (2003)655-665.

[28] S. Karthikeyan, B. Sivakumar and N. Sivakumar Film and Pore Diffusion Modeling for Adsorption of Reactive Red 2 from Aqueous Solution on to Activated Carbon Prepared from Bio-Diesel Industrial Waste E-Journal of Chemistry , 7(S1) (2010) S175-S1.

[29] N. A. Oladoja, I. O. Asia, C. O. Aboluwoye, Y. B. Oladimeji, A. O. Ashogbon. Studies on the Sorption of Basic Dye by Rubber (Hevea brasiliensis) Seed Shell. Turkish J Eng Env Sci, 32, (2008), 143-152.